ACS Photonics

pubs.acs.org/journal/apchd5

Article

Subcycle Mid-Infrared Electric-Field-Driven Scanning Tunneling Microscopy with a Time Resolution Higher Than 30 fs

Yusuke Arashida, Hiroyuki Mogi, Masashi Ishikawa, Ippo Igarashi, Akira Hatanaka, Naoki Umeda, Jinbo Peng, Shoji Yoshida, Osamu Takeuchi, and Hidemi Shigekawa*

Cite This: *ACS Photonics* 2022, 9, 3156−3164

Read Online

ACCESS | Metrics & More | Article Recommendations | Supporting Information

ABSTRACT: Electric-field-driven scanning tunneling microscopy (STM) that uses carrier envelope phase-controlled pulses in the THz region (THz-STM) has been attracting considerable attention because of its capability of probing ultrafast dynamics in materials. However, since the electric field is in the THz region, its time resolution of about 1 ps limits the range of measurable targets. Therefore, to pave the way for studying the local dynamics of non-equilibrium states such as elementary excitations and phase transitions in condensed materials, it is desirable to develop an STM system with a higher time resolution. Here, we report a mid-infrared (MIR) electric-field-driven STM system enabling an atomic-scale pump−probe method to be used over a wide range of time with a time resolution higher than 30 fs. We demonstrate the high potential of the new MIR-STM system by visualizing the photo-induced ultrafast non-equilibrium dynamics in $MoTe_2$. We succeeded in measuring ultrafast carrier dynamics in the time range of 0 to over 1 ps, which were well explained by the change in band structure associated with the carrier dynamics. In addition to time-resolved signal measurement, atomically resolved MIR-STM imaging was also realized.

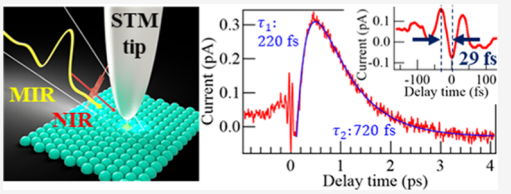

KEYWORDS: *STM, subcycle electric field, mid-infrared, electric-field driven, pump-probe technique, time-resolved STM*

INTRODUCTION

Understanding and controlling the ultrafast dynamics in non-equilibrium states of condensed materials are important for both basic and applied science and technologies.[1−4] Experiments using angle-resolved photoemission spectroscopy and diffraction methods with time resolutions in the femtosecond region have been actively conducted, and excellent results have been obtained.[5−10] However, these results and discussions are basically for the reciprocal lattice space. Since these dynamics are not spatially uniform but are strongly affected by local structures such as atomic-level defects, for further advancements, it is highly desirable to analyze these dynamics in real space while considering the surrounding effects of local structures.

Scanning tunneling microscopy (STM) has an atomic-scale resolution and is capable of evaluating local electronic structures in comparison with environmental structures.[11] However, since the time resolution of STM is in the sub-millisecond range, it is difficult to probe the dynamics of the ultrafast phenomena described above, and many attempts have been made to add a high time resolution since its invention.[12,13] The two methods considered as means of increasing time resolution dated from the earliest STM studies are to instantaneously give conductivity to the STM circuit using an ultrafast optical switch and to control the bias voltage applied between the STM tip and the sample using high-speed electronics.[14−17] The latter has been successfully used to measure spin dynamics in single-atomic-level research,[18−20] but the temporal resolution obtained using electronics is basically limited to the sub-nanosecond region.

Under these circumstances, an STM system with a time resolution in the femtosecond region was developed by combining STM with the optical pump−probe method used in ultrashort-pulse laser technologies.[21−23] Similar to the optical pump−probe method, the STM system uses the absorption bleaching mechanism,[23−25] thereby its time resolution determined by the laser pulse width is in the femtosecond region. Local spin dynamics have also been measured with this method.[26,27] Another method is electric-field-driven STM, which uses a carrier envelope phase (CEP)-controlled light source to produce a near-field to apply an instantaneous electric field between the STM tip and the sample.[28] This method substitutes the high-speed electronics with an electric field to enable a faster control of the bias voltage between the STM tip and the sample. When a THz electric field is used, this method is called THz-STM.[28−38]

In electric-field-driven STM, the change in tunnel current corresponding to the change in bias voltage is measured. Therefore, although care is required in analysis because the

Received: June 28, 2022
Published: September 2, 2022

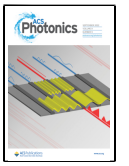

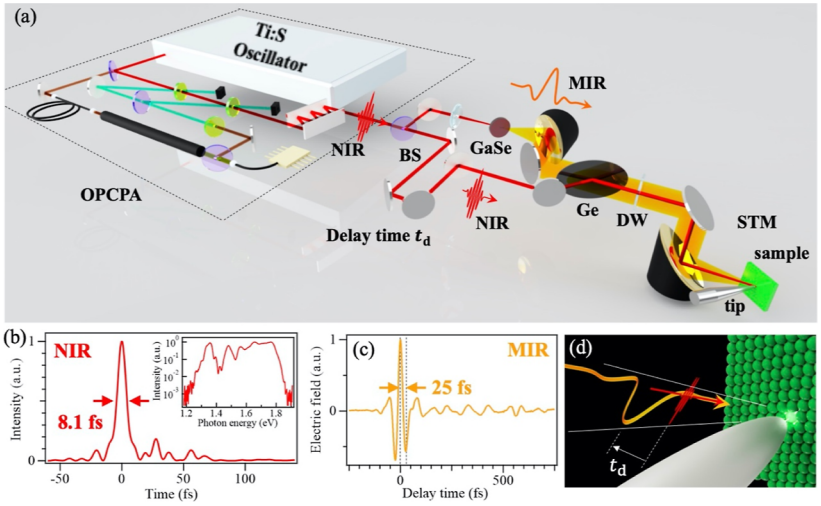

Figure 1. (a) Schematic diagram of the time-resolved MIR-STM system. BS: beam splitter, DW: diamond window, MIR: mid-infrared electric field E_{MIR}, and NIR: near-infrared electric field E_{NIR}. (b) Temporal profile of the output of the NIR pulse obtained by D-scan and its spectrum. (c) E_{MIR} waveform measured by using a photoconductive antenna (PCA) outside the STM chamber. (d) Schematic diagram of the measurement setup. The tunnel gap is irradiated by the combination of E_{MIR} and E_{NIR} with delay time t_d, and the corresponding change in tunnel current $I(t_d)$ is measured to obtain a time-resolved signal.

electric-field waveform is not a square, it is possible to measure the transient local density of states (LDOSs) of materials similar to that in normal STM,[28,32,33] making this method attractive. However, since its time resolution is determined by the bandwidth of the electric field used, the time resolution of THz-STM is limited to the 1 ps range, which is insufficient to analyze the non-equilibrium electronic dynamics.[8]

An attempt was made to develop a light source over a wider THz region to improve the time resolution; however, the obtained pulse width of the near-field was several hundred femtosecond.[39] The transition process in the attosecond region has recently been observed by using CEP-controlled pulses in the near-infrared (NIR) region.[40] However, since the mechanism of this system is based on the interference between two pulses of 6 fs width, unlike other laser-combined STM systems, its range of application is limited. Recently, scanning near-field optical microscopy (SNOM) techniques with a time resolution of 100 fs level have been reported.[41−43] Since SNOM measures permittivity of materials, we can obtain optically important local information. However, it is difficult to directly measure transient LDOSs. Therefore, the development of an electric-field-driven STM with a higher time resolution is strongly desired.

Here, we demonstrate electric-field-driven STM realized using CEP-controlled MIR pulses (MIR-STM) with a time resolution higher than 30 fs. Using the pump−probe method with a coaxial arrangement of the MIR beam and an NIR beam of 8 fs, we have succeeded in observing the photo-induced ultrafast nonequilibrium dynamics in $MoTe_2$ in the time range of 0 to over 1 ps with atomically resolved STM images.

EXPERIMENTAL SECTION

Time-Resolved MIR-STM System. Figure 1a shows a schematic diagram of our newly developed MIR-STM system. A Ti:S-based optical parametric chirped-pulse amplifier (Venteon OPCPA, Laser Quantum) was used as the primary light source of the NIR electric field $E_{NIR}(t)$.[44] The wavelength range of $E_{NIR}(t)$ was 660−940 nm, the pulse width was 8.1 fs, the pulse energy was 1 μJ, and the repetition frequency was 4 MHz (Figure 1b). A pair of chirp mirrors or a BK7 plates was used for fine adjustment to compensate for the dispersion of the fundamental wave (not shown in the figure). A wideband MIR pulse $E_{MIR}(t)$ was generated by the optical rectification effect by splitting the fundamental wave with a beam splitter (BS) and leading one of the beams to a GaSe crystal with a thickness of 30 μm.[45] After that, the basic light that was not wavelength-converted was removed from the MIR beam by passing the output from the GaSe crystal through a Ge plate.

The other NIR beam was passed through an optical delay stage (delay) and then reflected on a Ge plate to combine it with the MIR beam in a coaxial arrangement for pump−probe measurement, making it easy to adjust the optical system. Figure 1c shows the waveform of $E_{MIR}(t)$ obtained by using a photoconductive antenna (PCA) outside the STM chamber. Unipolar subcycle pulses with asymmetry between the positive and negative regions were produced, the half period of which was about 25 fs. The coaxial light beams were introduced into an ultrahigh-vacuum STM chamber (5×10^{-8} Pa) through a polycrystalline diamond window (DW in Figure 1a, φ = 12.7 mm) and focused onto the STM tip apex using an off-axis parabolic mirror (f = 15 mm) at an incident angle of 55°. Both the MIR and NIR beams were p-polarized with respect to the sample.

A mechanically polished Pt/Ir tip and a $MoTe_2$ sample were used for the STM measurement. It was confirmed that the thermal expansion problem could be negligible even when the pump−probe measurement was carried out with the intensity modulation of MIR light (see Figure S1 for details). Figure 1d shows a schematic diagram of the MIR-STM measurement. The tunnel gap was irradiated by the combination of $E_{MIR}(t)$ and $E_{NIR}(t)$ with a delay time t_d for the pump−probe method, and the change in tunnel current $I(t_d)$ was measured to obtain a time-resolved signal, similar to that in THz-STM.

RESULTS AND DISCUSSION

Evaluation of the MIR Near-Field. When the tunnel gap is irradiated by $E_{MIR}(t)$, an MIR near-field $E_{NF,MIR}(t)$ is produced at the tip apex via the mechanism of tip-induced

https://doi.org/10.1021/acsphotonics.2c00995
ACS Photonics 2022, 9, 3156−3164

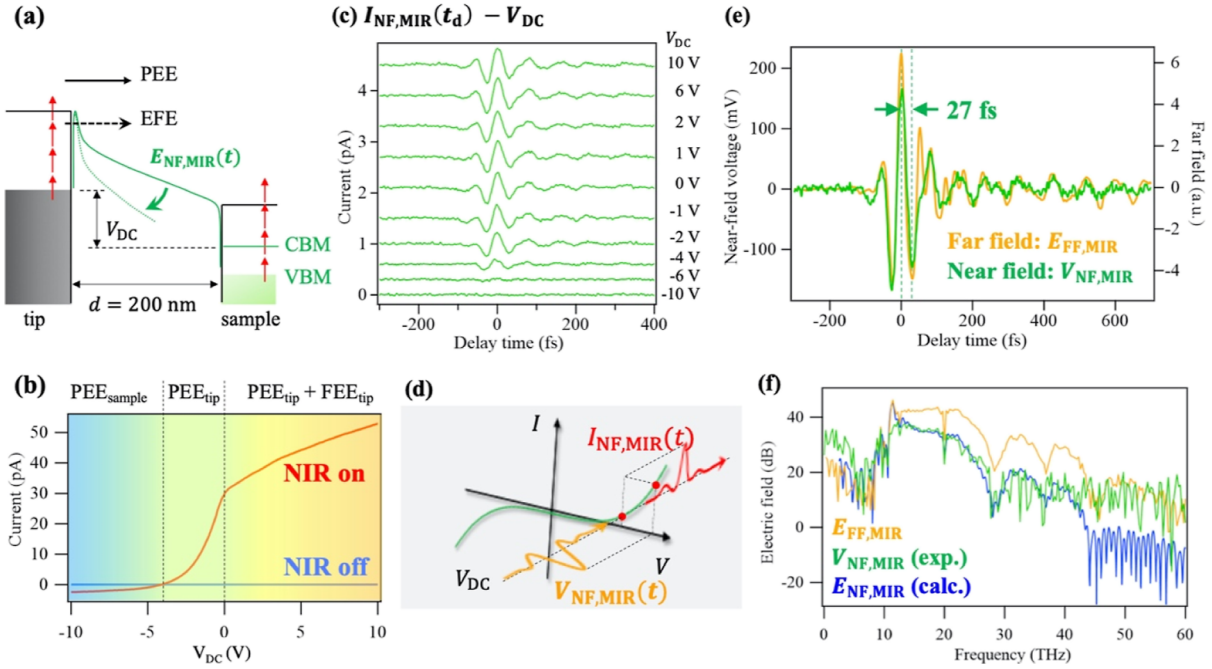

Figure 2. Evaluation of the MIR near field. (a) Energy diagram of the tunnel gap. Here, a bias voltage V_{DC} is applied between the STM tip and the sample. d is the tip-sample distance. CBM and VBM represent the conduction band minimum and valence band maximum, respectively. PEE and FEE denote photoemission electrons due to NIR light irradiation and field-effect-emitted electrons, respectively. $E_{NF,MIR}(t)$ is the MIR near-field produced on the STM tip via the mechanism of tip-induced enhancement of $E_{MIR}(t)$. (b) V_{DC} dependence of I = PEE + FED with NIR light irradiation and the MIR light turned off. (c) V_{DC} dependence of $E_{NF,MIR}(t)$-induced current $I_{NF,MIR}(t)$. The MIR beam was turned on and off at frequency of about 520 Hz with an optical chopper, and $I_{NF,MIR}(t)$ was measured by the lock-in detection method. (d) Relationship between the near-field voltage $V_{NF,MIR}(t)$ produced by $E_{NF,MIR}(t)$ and $I_{NF,MIR}(t)$, shown in (c) (see Figure S3 for details). (e) $E_{FF,MIR}(t)$, far-field $E_{MIR}(t)$ measured by the PCA at the tip position (yellow, see Figure S2 for details) and $V_{NF,MIR}(t)$ (green). $V_{NF,MIR}(t)$ was calculated using the shape of $I_{NF,MIR}(t)$ at 6 V shown in Figure 3c. (f) Far-field (yellow) and near-field (green) Fourier spectra obtained from the data in (e). The spectrum of $E_{NF,MIR}(t)$ calculated by the finite-difference time-domain (FDTD) method is also shown (blue, see Figure S4 for details).

enhancement.[42,46] The transient bias voltage $V_{NF,MIR}(t)$ formed by $E_{NF,MIR}(t)$ dynamically opens the STM circuit to detect the time-resolved signal. Therefore, it is important to evaluate $V_{NF,MIR}(t)$ under the measurement conditions. First, we confirmed using a photoconductive antenna (PCA) that $E_{MIR}(t)$ measured outside the STM chamber (Figure 1c) was well reproduced at the tunnel gap (see Figure S2 for details).

Next, we evaluated $E_{NF,MIR}(t)$ produced by $E_{MIR}(t)$. Figure 2a shows the energy diagram of the tunnel gap. Here, a sample bias voltage V_{DC} is applied between the STM tip and the sample (with the tip side grounded). Owing to the difference in the band structure between the tip and the sample, the vacuum level on the sample side is as low as ∼0.5 to ∼1 eV, even when V_{DC} is zero.[47,48] During the irradiation of the tunnel gap with the NIR light, with a tip-sample distance d of 200 nm to suppress the tunnel current, the current I = PEE + FEE was measured, where PEE and FEE represent the photoemission electrons and field-effect-emitted electrons, respectively. Figure 2b shows the $I-V_{DC}$ curve obtained by changing V_{DC} from −10 to 10 V. No current was generated when the NIR light was turned off (blue line), whereas $I(V_{DC})$ appeared by irradiating the tunnel gap with the NIR light (red line).

Since field emission is unlikely to occur on the flat sample surface, $I(V_{DC})$ observed for $V_{DC} < 0$ is due to PEE. At -4 V < $V_{DC} < 0$ V, photoemission electrons from the tip PEE_{tip} are the main component. Namely, the rapid change in $I(V_{DC})$ shows the change in $PEE_{tip}(V_{DC})$, which is excited by the light component on the high-energy side of $E_{MIR}(t)$, as shown in Figure 1b. The negative current at $V_{DC} < -4$ V is considered to be the photoelectrons from the sample surface, PEE_{sample}. The change in $I(V_{DC})$ observed for 0 V < V_{DC} is the change in $FEE_{tip}(V_{DC})$ because PEE_{tip} does not depend on V_{DC}.

We used this mechanism to evaluate $E_{NF,MIR}(t)$. When the tunnel gap is irradiated with MIR pulses, the barrier height at the tip apex changes, owing to $E_{NF,MIR}(t)$. Since the number of FEE_{tip} depends on the barrier height and the relaxation of hot electrons is faster than the change in $E_{NF,MIR}(t)$, the $E_{NF,MIR}(t)$ waveform can be evaluated by measuring the change in $I_{NF,MIR}(t_d)$, as similarly carried out in THz-STM.[32,34] Figure 2c shows the V_{DC} dependence of $I_{NF,MIR}(t_d)$, which appears to well reproduce the shape of $E_{MIR}(t)$ shown in Figure 1c, as expected. The appearance of the waveform for -4 V < $V_{DC} < 0$ V indicates that PEE_{tip} is affected by $E_{NF,MIR}(t)$. The momentum of these photoelectrons are strongly modified near the tip apex within several 10 fs[49] because the velocity of them is in the order of 1 nm/fs. In our experiment, $V_S = V_{DC} + V_{NF,MIR}(t)$ is applied to sample with the $I-V$ curve, as shown in Figure 2b, and the change in $I_{NF,MIR}(t_d)$ is measured, as shown in Figure 2d. We do not know $V_{NF,MIR}(t)$ at this point because $E_{NF,MIR}(t_d)$ may be different from $E_{MIR}(t_d)$. Therefore, to obtain an accurate $E_{NF,MIR}(t_d)$ waveform, it is necessary to calculate it from the $I_{NF,MIR}(t_d)$ shape shown in Figure 2c in consideration of the characteristics of the $I-V$ curve (see Figure S3 for details). Figure 2e shows $E_{MIR}(t)$ measured by the PCA at the tip position (yellow, see Figure S2 for detail) and $V_{NF,MIR}(t)$ (green) obtained from the calculation described above (see Figure S3 for detail). Figure 2f shows far-field (yellow) and near-field (green) Fourier spectra obtained from

https://doi.org/10.1021/acsphotonics.2c00995
ACS Photonics 2022, 9, 3156−3164

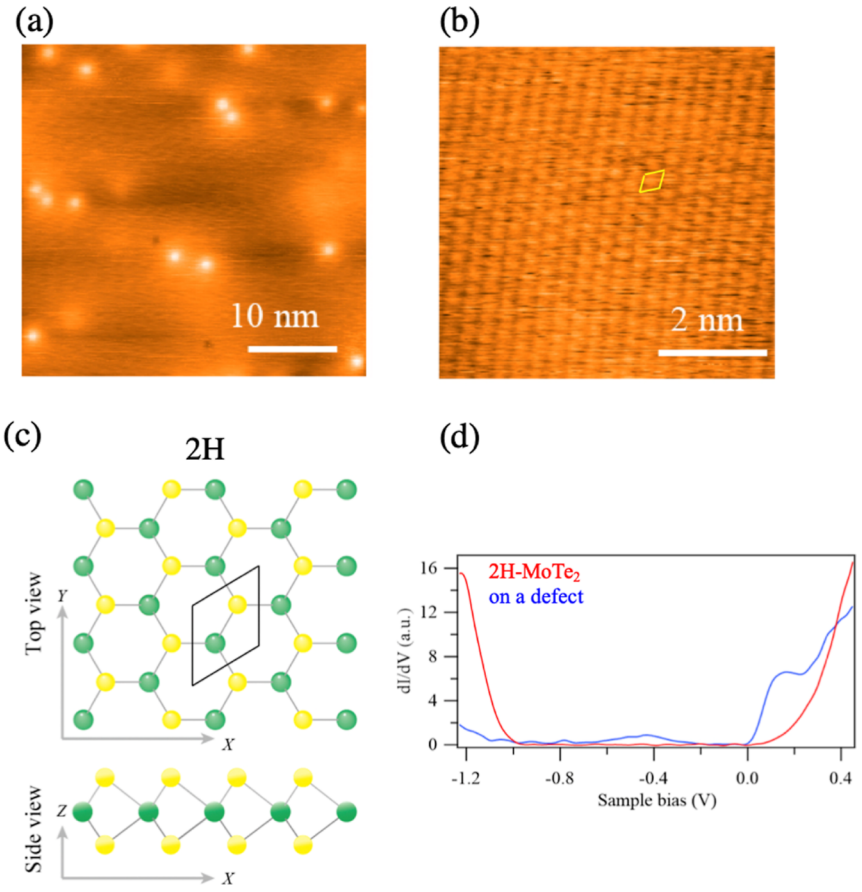

Figure 3. (a) Large-scale STM image of 2H−$MoTe_2$. Bright spots are oxidized defects. (b) STM image of 2H−$MoTe_2$ in an area without defects. (c) Schematic structures of 2H−$MoTe_2$ phases. (d)Typical I−V curves measured in areas with (blue) and without (red) defects. STM image taken after NIR light irradiation (30.6 kW/cm^2, 30 ms). TGB: twin grain boundary. Inset is the magnification of the 1T′ area. STM images were taken with the conditions of V_{DC} = 0.6 V and I = 50 pA.

the data in Figure 2e. The spectrum of $E_{NF,MIR}(t)$ calculated by the finite-difference time-domain (FDTD) method is also shown (blue, see Figure S4 for details). The difference observed between $E_{MIR}(t)$ and $V_{NF,MIR}$ (t) indicates the importance of confirming the shape of $E_{NF,MIR}(t)$ before measurement, as we have pointed out in a previous paper.[32]

Time-Resolved MIR-STM Measurement. *Sample Preparation.* 2H−$MoTe_2$, a transition-metal dichalcogenide (TMDC),[50] was used as a sample. In a previous study of $MoTe_2$ using a THz-STM system, in which the time resolution was 1 ps, carrier recombination dynamics of 18 and 606 ps were observed, but the processes faster than 1 ps were beyond its measurement limit.[32] However, important non-equilibrium dynamics, such as the modulation of the band structure associated with ultrafast electron dynamics, appear at <∼1 ps.[51] Thus, $MoTe_2$ is considered to be suitable for demonstrating the performance of the newly developed MIR-STM system. However, $MoTe_2$ exhibits a large electron lattice interaction among the TMDCs and forms phases such as semiconducting, metallic, charge density wave (CDW), and superconducting phases depending on its crystal structure and conditions.[52,53] Therefore, to probe the ultrafast electronic dynamics without such structural changes which make analysis complicated, the NIR light intensity was sufficiently reduced to 0.56 mW measured externally, 1 order lower than that used in ref 24. To confirm the suitability of the conditions, we carried out time-resolved MIR-STM imaging as will be explained in detail later.

A clean surface was obtained by exfoliating bulk 2H−$MoTe_2$ fixed with a conductive adhesive on a copper substrate in an ultrahigh-vacuum (2×10^{-8} Pa) preparation chamber. Then, it was moved to the STM measurement chamber (5×10^{-8} Pa) and cooled to 78 K, and experiments were performed. 2H−$MoTe_2$ has a hexagonal symmetric crystal structure, and the bulk crystal is a semiconductor with a band gap of ∼1.0 eV at 77 K.[54] Figure 3a shows a typical STM image of 2H−$MoTe_2$. Bright spots are oxidized defects.[32] Figure 3b shows an STM image of 2H−$MoTe_2$ with atomic resolution obtained in the area without defects. A schematic structure of 2H−$MoTe_2$ is shown in Figure 3c. Figure 3d shows typical dI/dV curves obtained in the areas with (blue) and without (red) defects. Defect-related gap states are observed for the former, and time-resolved MIR-STM measurements were carried out in the area without defects to avoid their effects.

Measurement and Analysis. After choosing an area without defects by STM observation, time-resolved MIR-STM measurements were performed at 78 K, as shown in Figure 1d. For the time-resolved STM measurement, a pump−probe method was performed using NIR pulsed light as an excitation and MIR light as a probe. The MIR light was turned on and off at a frequency of 520 Hz, and the modulated tunnel current $I_{t,MIR}(t_d)$ was detected as the time-resolved MIR-STM signal by the lock-in detection method, while STM feedback was

https://doi.org/10.1021/acsphotonics.2c00995
ACS Photonics 2022, 9, 3156−3164

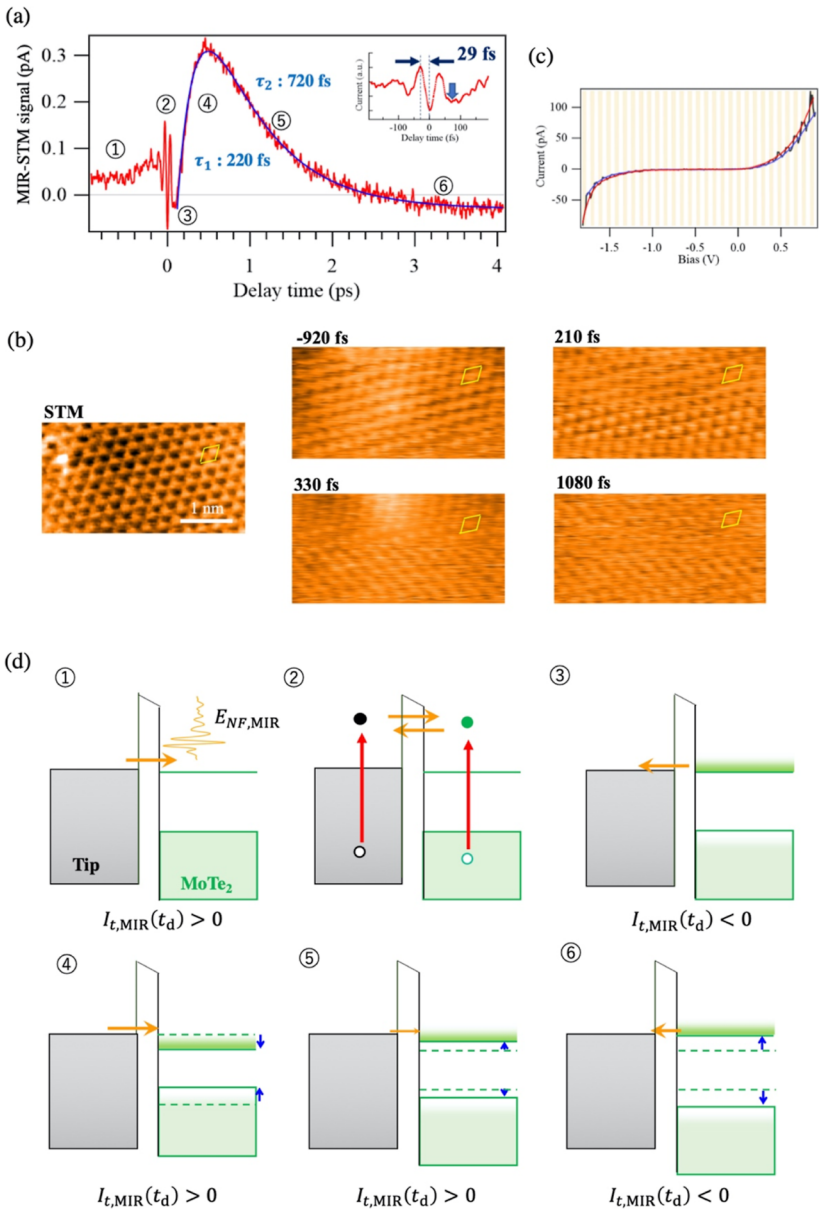

Figure 4. (a) Time-resolved MIR-STM signal obtained in the area without defects (V_{DC} = 150 mV, I = 50 pA, NIR pulse: 0.56 mW outside). MIR light was turned on and off at a frequency of 520 Hz for the lock-in detection. The inset is a magnification of the signal around t_d = 0. The blue line indicates the fitting curve obtained using an exponential function with two components. (b) High resolution STM image of 2H−$MoTe_2$ shown in Figure 3b and time-resolved MIR-STM images obtained for delay times t_d of −920, 210, 330, and 1080 fs (4 × 4 nm^2, V_{DC} = 31 mV, I = 40 pA, scan speed: 1.5 s/nm). (c) Result of light-modulated scanning tunneling spectroscopy (LM-STS).[55,56] The I−V curve was measured while turning the NIR beam on and off at a frequency of 40 Hz (V_{DC} = 800 mV, I = 50 pA, 0.56 mW outside, 512 points/0.82 s). By drawing the envelopes of the signal, two I−V curves for with (red) and without (blue) light irradiation were obtained simultaneously. (d) Schematic band structures explaining the time-resolved signal shown in (a).

carried out using the total tunnel current. Since V_{DC} is small and $E_{NF,MIR}(t)$ is not completely monopolar, the direction of the MIR-STM tunnel current signal at $t = t_d$, $I_{t,MIR}(t_d)$ changes from the STM tip to the sample $[I_{t,MIR}(t_d) > 0]$ and from the sample to the STM tip $[I_{t,MIR}(t_d) < 0)]$, depending on the direction of the bias voltage $V_S(t) = V_{DC} + V_{NF,MIR}(t)$. Since $V_{NF,MIR}$ is not a rectangular wave, $I_{t,MIR}(t_d)$ is an integral over the waveform. The relationship between the electric field $E_{NF,MIR}$ and the STM gap is shown in ① in Figure 4d.

Figure 4a shows a typical result. In the region of $t_d > 0$, a rapid increase in signal intensity ($t_d < 0.5$ ps) and its relaxation were observed. This is the first ever time-resolved STM signal obtained in the time range of 0 to 1 ps. The observed change in $I(t_d)$ in the first 1 ps is produced by the tunneling of electrons near the Fermi level between the STM tip and the sample, namely, the ultrafast dynamics occurring in the $MoTe_2$ sample were successfully probed. The blue line in Figure 4a shows the result of fitting with the double exponential function $g_1\exp\left(-\frac{t}{\tau_1}\right) + g_2\exp\left(-\frac{t}{\tau_2}\right)$ where g_1 and g_2 are constants showing the intensity of each function. A rise at τ_1 = 220 fs followed by a decay at τ_2 = 720 fs was obtained.

As described above, to avoid the structural changes due to photoexcitation, the NIR light intensity was sufficiently reduced. To confirm the suitability of the conditions, we carried out time-resolved MIR-STM imaging. Figure 4b shows

https://doi.org/10.1021/acsphotonics.2c00995
ACS Photonics 2022, 9, 3156−3164

a high-resolution STM image and MIR-STM images obtained at t_d = −920, 210, 330, and 1080 fs. The STM tip was scanned from left to right and from bottom to top. Since measurements were carried out under light irradiation, there were some fluctuations, and the resolution slightly changed during scanning. As shown in the figures, however, atomically time-resolved STM images during the ultrafast photo-induced dynamics in $MoTe_2$ were successfully obtained for the first time. A small hexagonal structure, including the second layer, can be observed in places where the resolution is high for both STM and MIR-STM images.

Although the appearance of 2H−$MoTe_2$ may differ depending on the resolution, its structure was basically maintained, as can be seen from the unit cell. Namely, it was confirmed that the electronic state dynamics were measured while maintaining the stability of the sample structure. This is the first time-resolved STM observation of ultrafast dynamics in the <1 ps region.

We next discuss in detail how to interpret the observed ultrafast phenomena. First, we carried out light-modulated scanning tunneling spectroscopy (LM-STS) measurements[55,56] to examine the band structure. Figure 4c shows the result of the LM-STS measurement obtained in the area without defects. The $I-V$ curve was measured while turning the NIR beam on and off at a frequency of 40 Hz. By drawing the envelopes of the signal, two $I-V$ curves in cases with (red) and without (blue) light irradiation were obtained simultaneously. Almost no shift was observed between the $I-V$ curves obtained with and without NIR irradiation, indicating that band bending and photovoltage are not effective for this sample. No apparent structural changes were observed in the MIR-STM images, as shown in Figure 4b. It is considered that no phase transition accompanying structural changes occurred, owing to the decreasing photoexcitation intensity, as expected.

A possible mechanism to explain the MIR-STM signal observed in Figure 4a is band gap renormalization, which is a phenomenon where the band gap changes with increasing carrier density. There are some reports on experiments and theoretical analyses of this phenomenon.[57,58] In the case of a few-layer MoS_2 sample with a band gap of 1.8 eV, the changes in the band structure of MoS_2 due to resonant excitation (1.83 eV) and nonresonant excitation (3.10 eV) were analyzed.[59] In the nonresonant case, the band gap first shrank in the range of several 100 fs and then relaxed on the order of ∼1 ps. The shrinkage is due to the relaxation of the excited electrons to the conduction band edge, resulting in the appearance of the screening effect. Subsequent relaxation was attributed to the reduction of the screening effect due to the formation of a bound state (e.g., excitons). The shrinkage magnitude increased with the photoexcitation light intensity, reaching about −30 meV at 110 $\mu J/cm^2$. In our system, the excitation energy is ∼1.5 eV. Considering that the band gap of $MoTe_2$ is ∼1 eV, our experimental conditions correspond to the nonresonant excitation case in the ref 57. In addition, since the photoexcitation light intensity is approximately 50 $\mu J/m^2$ and there is a tip enhancement effect, the band shrinkage is considered equal to or larger than that in our experiment.

In a report on $MoTe_2$,[51] for example, the change in transmittance of the probe light after excitation at 800 nm and the time evolution of the absorption spectrum after excitation at 800 nm were analyzed. The former showed changes in the rising part at 100−140 fs depending on the pump light intensity. In the latter, the red-shifted gap after excitation relaxed on the order of 1 ps. Another study on $MoTe_2$ was carried out on the basis of the measurement of absorption spectra between the core level and the conduction/valence band after pumping light of 800 nm on the sample.[57] The position of the red-shifted conduction band edge changed to the high-energy side in the <1 ps region.

The timescales of the dynamics in these previous studies correspond well to the results of our MIR-STM experiments. In STM, the tunnel current appears positive or negative depending on the relationship between the Fermi levels in the STM tip and the sample. Therefore, the sign of the tunnel current can be used as an index for evaluating the changes in the sample band structure.

To consider the signal in Figure 4a in detail, it is divided into areas ① to ⑥. Figure 4d shows model diagrams explaining the signal in each region. First, in area ① of t_d < 0 at the left of the figure, $I_{t,MIR}(t_d) > 0$. STM measurements were performed under feedback conditions with sample bias V_S = 31 mV. Therefore, the integral value of the tunnel current that gives the MIR-STM signal became positive, owing to the relationship between the shape of the $I-V$ curve and the MIR waveform.

Next, in the vicinity of t_d = 0 (area ② in Figure 4a), the waveform of the near field shown in Figure 2e is reproduced by a signal of the tunnel current. This is due to the NIR-photoexcited hot electrons tunneling between the STM tip and the sample, reflecting the change in the tunnel barrier in response to the MIR waveform ($E_{NF,MIR}$) when the NIR pulse overlaps with the MIR pulse (② in Figure 4d), similar to the case of THz-STM.[32] This indicates that the relaxation of the hot electrons excited by the NIR light occurs within a time shorter than the NIR pulse width of 8 fs. Now tunnel current is expected to be controlled ultra-fast and phase-sensitive.[29]

However, as shown by the arrow in the inset of Figure 4a, the negative $I_{t,MIR}(t_d)$ signal continued from around t_d = 60 fs, deviating from the MIR waveform. This is because the hot electrons relax and accumulate in the CBM, then tunnel to the tip side [③ in Figure 4d]. As t_d increases, the number of electrons that accumulated in the CBM increases, which initiates band gap renormalization (band gap reduction and subsequent relaxation). Band gap renormalization is caused by the screening of the electric field by electrons accumulated in the CBM and energy transfer from electrons to the sample lattice.[51,60] This process is represented by ④ to ⑥ in Figure 4d. Previous studies have shown that the relaxation time of nonresonantly excited hot electrons to CBM by electron−phonon interaction was in the range of several 100 fs,[51] which corresponds well to our result. The time scale of the reduction of the screening effect due to the formation of a bound state was predicted to be on the order of 1 ps in a previous study,[60] which is consistent with the decay time of the tunnel current in this study, τ_2 = 720 fs. Since we chose defect-free sites, the exciton formation process is more likely, but these effects may be site-dependent.

In area ⑥, $I_{t,MIR}(t_d) < 0$ again. The direction of the tunnel current is changed by the flow of electrons that accumulated in the CBM with the relaxation of band renormalization. After that, the electron density in the CBM decreases, owing to such as electron−hole recombination, and the signal returns to the initial state ①. This process corresponds to the long relaxation time previously observed with THz-STM. For a sample with photovoltage, the effect of band bending must be considered.

https://doi.org/10.1021/acsphotonics.2c00995
ACS Photonics 2022, 9, 3156−3164

As described above, the ultrafast dynamics after 8 fs NIR light irradiation were observed using by time-resolved MIR-STM. We succeeded in measuring ultrafast carrier dynamics in the <1 ps region, which was well explained by the change in the band structure associated with the carrier dynamics. In addition to the time-resolved signal measurement, time-resolved imaging was also realized. We have shown that MIR-STM is a very promising method. It is expected that a more detailed analysis including photo-induced phase transitions will be possible if the interaction between the electron system and phonons is directly observed. The development of a method for the detailed analysis of transient $I-V$ curves is also strongly desired for studies in the energy space to progress further. However, electric-field-driven time-resolved STM uses subcycle pulses instead of square waves, as instantaneously applied bias voltages: therefore, a more detailed analysis is required to obtain correct $I-V$ curves. Studies have been carried out using THz-STM,[32,33] but this method has not yet been established. If MIR-STM realizes the evaluation of transient $I-V$ curves, it will be possible to analyze the dynamics of the electronic structures in ultrafast phenomena in the <30 fs region in real space. Since these analyses are beyond the scope of this study, we leave them for future work. The combination of the developed system we demonstrated in this paper with a THz electric field is expected to open a new possibility.[61]

CONCLUSIONS

We have realized the first ever mid-infrared (MIR) electric-field-driven STM system enabling the pump−probe method to be used over a wide time range with a time resolution higher than 30 fs. We demonstrated the high potential of the new MIR-STM system by visualizing ultrafast nonequilibrium carrier dynamics induced by the irradiation of a sample with an NIR pulse of 8 fs width. We succeeded in measuring ultrafast carrier dynamics in the range of 0 to over 1 ps which were well explained by the change in band structure associated with the carrier dynamics. In addition to time-resolved signal measurement, time-resolved imaging was also realized. It is highly expected that this method will pave the way for studying the local dynamics of non-equilibrium states such as elementary excitations and phase transitions in condensed materials.

ASSOCIATED CONTENT

Supporting Information

The Supporting Information is available free of charge at https://pubs.acs.org/doi/10.1021/acsphotonics.2c00995.

Analysis of thermal expansion problem; evaluation of MIR far-field; reconstruction of the near field voltage $V_{NF,MIR}(t)$ from $I_{NF,MIR}(t)$; FDTD calculation of MIR near-field waveform (PDF)

AUTHOR INFORMATION

Corresponding Author

Hidemi Shigekawa − *Faculty of Pure and Applied Sciences, University of Tsukuba, Tsukuba 305-8573, Japan;* orcid.org/0000-0001-9550-5148; Email: hidemi@ims.tsukuba.ac.jp

Authors

Yusuke Arashida − *Faculty of Pure and Applied Sciences, University of Tsukuba, Tsukuba 305-8573, Japan*

Hiroyuki Mogi − *Faculty of Pure and Applied Sciences, University of Tsukuba, Tsukuba 305-8573, Japan*

Masashi Ishikawa − *Faculty of Pure and Applied Sciences, University of Tsukuba, Tsukuba 305-8573, Japan*

Ippo Igarashi − *Faculty of Pure and Applied Sciences, University of Tsukuba, Tsukuba 305-8573, Japan*

Akira Hatanaka − *Faculty of Pure and Applied Sciences, University of Tsukuba, Tsukuba 305-8573, Japan*

Naoki Umeda − *Faculty of Pure and Applied Sciences, University of Tsukuba, Tsukuba 305-8573, Japan*

Jinbo Peng − *Faculty of Pure and Applied Sciences, University of Tsukuba, Tsukuba 305-8573, Japan*

Shoji Yoshida − *Faculty of Pure and Applied Sciences, University of Tsukuba, Tsukuba 305-8573, Japan*

Osamu Takeuchi − *Faculty of Pure and Applied Sciences, University of Tsukuba, Tsukuba 305-8573, Japan*

Complete contact information is available at: https://pubs.acs.org/10.1021/acsphotonics.2c00995

Author Contributions

Y.A. developed the system, and took data with M.I., I.I., A.H., and N.U. J.P., S.Y. and O.T. provided technical advice. H.S. organized and supervised the project and edited the paper with Y.A. and S.Y.

Funding

We acknowledge the financial support of a grant-in-aid for Scientific Research (17H06088, 20H00341, 20H05662) from Japan Society for the Promotion of Science.

Notes

The authors declare no competing financial interest.

REFERENCES

(1) Shah, J. *Ultrafast Spectroscopy of Semiconductors and Semiconductor Nanostructures*; Springer, 1999.

(2) Petek, H.; Ogawa, S. Femtosecond time-resolved two-photon photoemission studies of electron dynamics in metals. *Prog. Surf. Sci.* **1997**, *56*, 239−310.

(3) Huber, R.; Tauser, F.; Brodschelm, A.; Bichler, M.; Abstreiter, G.; Leitenstorfer, A. How many-particle interactions develop after ultrafast excitation of an electron−hole plasma. *Nature* **2001**, *414*, 286−289.

(4) Giannetti, C.; Capone, M.; Fausti, D.; Fabrizio, M.; Parmigiani, F.; Mihailovic, D. Ultrafast optical spectroscopy of strongly correlated materials and high-temperature superconductors: a non-equilibrium approach. *Adv. Phys.* **2016**, *65*, 58−238.

(5) Rohwer, T.; Hellmann, S.; Wiesenmayer, M.; Sohrt, C.; Stange, A.; Slomski, B.; Carr, A.; Liu, Y.; Avila, L. M.; Kalläne, M.; Mathias, S.; Kipp, L.; Rossnagel, K.; Bauer, M. Collapse of long-range charge order tracked by time-resolved photoemission at high momenta. *Nature* **2011**, *471*, 490−493.

(6) Reimann, J.; Schlauderer, S.; Schmid, C. P.; Langer, F.; Baierl, S.; Kokh, K. A.; Tereshchenko, O. E.; Kimura, A.; Lange, C.; Güdde, J.; Höfer, U.; Huber, R. Subcycle observation of lightwave-driven Dirac currents in a topological surface band. *Nature* **2018**, *562*, 396−400.

(7) Wang, Y. H.; Steinberg, H.; Jarillo-Herrero, P.; Gedik, N. Observation of Floquet-Bloch States on the Surface of a Topological Insulator. *Science* **2013**, *342*, 453−457.

(8) Gierz, I.; Petersen, R. P.; Mitrano, K. L.; Cacho, A.; Turcu, A.; Springate, M.; Stöhr, A.; Köhler, A.; Starke, U.; Cavalleri, A. Snapshots of non-equilibrium Dirac carrier distributions in graphene. *Nat. Mater.* **2013**, *12*, 1119−1124.

(9) Morrison, V. R.; Chatelain, R. P.; Tiwari, K. L.; Hendaoui, A.; Bruhács, A.; Chaker, M.; Siwick, B. J. A photoinduced metal-like phase of monoclinic VO_2 revealed by ultrafast electron diffraction. *Science* **2014**, *346*, 445−448.
(10) Sokolowski-Tinten, K.; Blome, C.; Dietrich, C.; Tarasevitch, A.; Horn von Hoegen, M.; von der Linde, D.; Cavalleri, A.; Squier, J.; Kammler, M. Femtosecond x-ray measurement of ultrafast melting and large acoustic transients. *Phys. Rev. Lett.* **2001**, *87*, 225701.
(11) Binnig, G.; Rohrer, H.; Gerber, C.; Weibel, E. 7×7 Reconstruction on Si(111) Resolved in Real Space. *Phys. Rev. Lett.* **1983**, *50*, 120−123.
(12) Tian, Y.; Yang, F.; Guo, C.; Jiang, Y. Recent Advances in Ultrafast Time-Resolved Scanning Tunneling Microscopy. *Surf. Rev. Lett.* **2018**, *25*, 1−19.
(13) Terada, Y.; Yoshida, S.; Takeuchi, O.; Shigekawa, H. Laser-combined scanning tunnelling microscopy for probing ultrafast transient dynamics. *J. Phys. Condens. Matter* **2010**, *22*, 264008.
(14) Weiss, S.; Ogletree, D. F.; Botkin, D.; Salmeron, M.; Chemla, D. S. Ultrafast scanning probe microscopy. *Appl. Phys. Lett.* **1993**, *63*, 2567−2569.
(15) Nunes, G.; Freeman, M. R. Picosecond Resolution in Scanning Tunneling Microscopy. *Science* **1993**, *262*, 1029−1032.
(16) Moult, I.; Herve, M.; Pennec, Y. Ultrafast spectroscopy with a scanning tunneling microscope. *Appl. Phys. Lett.* **2011**, *98*, 233103.
(17) Saunus, C.; Raphael Bindel, B. J.; Pratzer, M.; Morgenstern, M. Versatile scanning tunneling microscopy with 120 ps time resolution. *Appl. Phys. Lett.* **2013**, *102*, 051601.
(18) Loth, S.; Etzkorn, M.; Lutz, C. P.; Eigler, D. M.; Heinrich, A. J. Measurement of Fast Electron Spin Relaxation Times with Atomic Resolution. *Science* **2010**, *329*, 1628−1630.
(19) Yan, S.; Choi, D. J.; Burgess, J. A. J.; Rolf-Pissarczyk, S.; Loth, S. Control of quantum magnets by atomic exchange bias. *Nat. Nanotechnol.* **2015**, *10*, 40−45.
(20) Friedlein, J.; Harm, J.; Lindner, P.; Bargsten, L.; Bazarnik, M.; Krause, S.; Wiesendanger, R. A radio-frequency spin-polarized scanning tunneling microscope. *Rev. Sci. Instrum.* **2019**, *90*, 123705.
(21) Li, S.; Chen, S.; Li, J.; Wu, R.; Ho, W. Joint Space-Time Coherent Vibration Driven Conformational Transitions in a Single Molecule. *Phys. Rev. Lett.* **2017**, *119*, 176002.
(22) Yoshida, S.; Yokota, M.; Takeuchi, O.; Oigawa, H.; Mera, Y.; Shigekawa, H. Single-Atomic-Level Probe of Transient Carrier Dynamics by Laser-Combined Scanning Tunneling Microscopy. *Appl. Phys. Express* **2013**, *6*, 032401.
(23) Terada, Y.; Yoshida, S.; Takeuchi, O.; Shigekawa, H. Real-space imaging of transient carrier dynamics by nanoscale pumpg-probe microscopy. *Nat. Photonics* **2010**, *4*, 869−874.
(24) Mogi, H.; Wang, Z. H.; Bamba, T.; Takaguchi, Y.; Endo, T.; Yoshida, S.; Taninaka, A.; Oigawa, H.; Miyata, Y.; Takeuchi, O.; Shigekawa, H. Development of laser-combined scanning multiprobe spectroscopy and application to analysis of $WSe_2/MoSe_2$ in-plane heterostructure. *Appl. Phys. Express* **2019**, *12*, 045002.
(25) Guo, C.; Meng, X.; Fu, H.; Wang, Q.; Wang, H.; Tian, Y.; Peng, J.; Ma, R.; Weng, Y.; Meng, S.; Wang, E.; Jiang, Y. Probing Nonequilibrium Dynamics of Photoexcited Polarons on a Metal-Oxide Surface with Atomic Precision. *Phys. Rev. Lett.* **2020**, *124*, 206801.
(26) Yoshida, S.; Aizawa, Y.; Wang, Z. H.; Oshima, R.; Mera, Y.; Matsuyama, E.; Oigawa, H.; Takeuchi, O.; Shigekawa, H. Probing ultrafast spin dynamics with optical pump-probe scanning tunnelling microscopy. *Nat. Nanotechnol.* **2014**, *9*, 588−593.
(27) Wang, Z. H.; Yoon, C. H.; Yoshida, S.; Arashida, Y.; Takeuchi, O.; Ohno, Y.; Shigekawa, H. Surface-mediated spin dynamics probed by optical-pump-probe scanning tunneling microscopy. *Phys. Chem. Chem. Phys.* **2019**, *21*, 7256−7260.
(28) Cocker, T. L.; Jelic, V.; Gupta, M.; Molesky, S. J.; Burgess, J. A. J.; Reyes, G. D. L.; Titova, L. V.; Tsui, Y. Y.; Freeman, M. R.; Hegmann, F. A. An ultrafast terahertz scanning tunnelling microscope. *Nat. Photonics* **2013**, *7*, 620−625.
(29) Yoshioka, K.; Katayama, I.; Minami, Y.; Kitajima, M.; Yoshida, S.; Shigekawa, H.; Takeda, J. Real-space coherent manipulation of electrons in a single tunnel junction by single-cycle terahertz electric fields. *Nat. Photonics* **2016**, *10*, 762−765.
(30) Wang, L.; Xia, Y.; Ho, W. Atomic-scale quantum sensing based on the ultrafast coherence of an H2 molecule in an STM cavity. *Science* **2022**, *376*, 401−405.
(31) Cocker, T. L.; Peller, D.; Yu, P.; Repp, J.; Huber, R. Tracking the ultrafast motion of a single molecule by femtosecond orbital imaging. *Nature* **2016**, *539*, 263−267.
(32) Yoshida, S.; Hirori, H.; Tachizaki, T.; Yoshioka, K.; Arashida, Y.; Wang, Z. H.; Sanari, Y.; Takeuchi, O.; Kanemitsu, Y.; Shigekawa, H. Subcycle Transient Scanning Tunneling Spectroscopy with Visualization of Enhanced Terahertz Near Field. *ACS Photonics* **2019**, *6*, 1356−1364.
(33) Jelic, V.; Iwaszczuk, K.; Nguyen, P. H.; Rathje, C.; Hornig, G. J.; Sharum, H. M.; Hoffman, J. R.; Freeman, M. R.; Hegmann, F. A. Ultrafast terahertz control of extreme tunnel currents through single atoms on a silicon surface. *Nat. Phys.* **2017**, *13*, 591−598.
(34) Yoshioka, K.; Katayama, I.; Arashida, Y.; Ban, A.; Kawada, Y.; Konishi, K.; Takahashi, H.; Takeda, J. Tailoring Single-Cycle Near Field in a Tunnel Junction with Carrier-Envelope Phase-Controlled Terahertz Electric Fields. *Nano Lett.* **2018**, *18*, 5198−5204.
(35) Luo, Y.; Jelic, V.; Chen, G.; Nguyen, P. H.; Liu, Y. J. R.; Calzada, J. A. M.; Mildenberger, D. J.; Hegmann, F. A. Nanoscale terahertz STM imaging of a metal surface. *Phys. Rev. B* **2020**, *102*, 205417.
(36) Yoshida, S.; Arashida, Y.; Hirori, H.; Tachizaki, T.; Taninaka, A.; Ueno, H.; Takeuchi, O.; Shigekawa, H. Terahertz Scanning Tunneling Microscopy for Visualizing Ultrafast Electron Motion in Nanoscale Potential Variations. *ACS Photonics* **2021**, *8*, 315−323.
(37) Ammerman, S. E.; Jelic, V.; Wei, Y.; Breslin, V. N.; Hassan, M.; Everett, N.; Lee, S.; Sun, Q.; Pignedoli, C. A.; Ruffieux, P.; Fasel, R.; Cocker, T. L. Lightwave-driven scanning tunnelling spectroscopy of atomically precise graphene nanoribbons. *Nat. Commun.* **2021**, *12*, 6794.
(38) Abdo, M.; Sheng, S.; Rolf-Pissarczyk, S.; Arnhold, L.; Burgess, J. A. J.; Isobe, M.; Malavolti, L.; Loth, S. Variable Repetition Rate THz Source for Ultrafast Scanning Tunneling Microscopy. *ACS Photonics* **2021**, *8*, 702−708.
(39) Müller, M.; Martín, S. N.; Kampfrath, T.; Wolf, M. Phase-Resolved Detection of Ultrabroadband THz Pulses inside a Scanning Tunneling Microscope Junction. *ACS Photonics* **2020**, *7*, 2046−2055.
(40) Garg, M.; Martin-Jimenez, A.; Pisarra, M.; Luo, Y.; Martín, F.; Kern, K. Real-space subfemtosecond imaging of quantum electronic coherences in molecules. *Nat. Photonics* **2021**, *16*, 196−202.
(41) Nishida, J.; Johnson, S. C.; Chang, P. T. S.; Wharton, D. M.; Dönges, S. A.; Khatib, O.; Raschke, M. B. Ultrafast infrared nano-imaging of far-from-equilibrium carrier and vibrational dynamics. *Nat. Commun.* **2022**, *13*, 1083.
(42) Eisele, M.; Cocker, T. L.; Huber, M. A.; Plankl, M.; Viti, L.; Ercolani, D.; Sorba, L.; Vitiello, M. S.; Huber, R. Ultrafast multi-terahertz nano-spectroscopy with sub-cycle temporal resolution. *Nat. Photonics* **2014**, *8*, 841−845.
(43) Plankl, M.; Faria Junior, P. E.; Mooshammer, F.; Siday, T.; Zizlsperger, M.; Sandner, F.; Schiegl, F.; Maier, S.; Huber, M. A.; Gmitra, M.; Fabian, J.; Boland, J. L.; Cocker, T. L.; Huber, R. Subcycle contact-free nanoscopy of ultrafast interlayer transport in atomically thin heterostructures. *Nat. Photonics* **2021**, *15*, 594−600.
(44) Yoshioka, K.; Igarashi, I.; Yoshida, S.; Arashida, Y.; Katayama, I.; Takeda, J.; Shigekawa, H. Subcycle mid-infrared coherent transients at 4 MHz repetition rate applicable to light-wave-driven scanning tunneling microscopy. *Opt. Lett.* **2019**, *44*, 5350.
(45) Kübler, C.; Huber, R.; Leitenstorfer, A. Ultrabroadband terahertz pulses: generation and field-resolved detection. *Semicond. Sci. Technol.* **2005**, *20*, S128−S133.
(46) Lu, F.; Jin, M.; Belkin, M. A. Tip-enhanced infrared nanospectroscopy via molecular expansion force detection. *Nat. Photonics* **2014**, *8*, 307−312.

https://doi.org/10.1021/acsphotonics.2c00995
ACS Photonics 2022, 9, 3156−3164

(47) Shimada, T.; Ohuchi, F. S.; Parkinson, B. A. Work Function and Photothreshold of Layered Metal Dichalcogenides. *Jpn. J. Appl. Phys.* **1994**, *33*, 2696−2698.
(48) Yu, E. T.; Barmak, K.; Ronsheim, P.; Johnson, M. B.; McFarland, P.; Halbout, J.-M. Two-dimensional profiling of shallow junctions in Si metal-oxide-semiconductor structures using scanning tunneling spectroscopy and transmission electron microscopy. *J. Appl. Phys.* **1996**, *79*, 2115.
(49) Herink, G.; Solli, D. R.; Gulde, M.; Ropers, C. Field-driven photoemission from nanostructures quenches the quiver motion. *Nature* **2012**, *483*, 190−193.
(50) Wang, Q. H.; Kalantar-Zadeh, K.; Kis, A.; Coleman, J. N.; Strano, M. S. Electronics and optoelectronics of two-dimensional transition metal dichalcogenides. *Nat. Nanotechnol.* **2012**, *7*, 699−712.
(51) Chi, Z.; Chen, H.; Zhao, Q.; Weng, Y. X. Ultrafast carrier and phonon dynamics in few-layer 2H-$MoTe_2$. *J. Chem. Phys.* **2019**, *151*, 114704.
(52) Wang, L.; Wu, Y.; Yu, Y.; Chen, A.; Li, H.; Ren, W.; Lu, S.; Ding, S.; Yang, H.; Xue, Q. K.; Li, F. S.; Wang, G. Direct Observation of One-Dimensional Peierls-type Charge Density Wave in Twin Boundaries of Monolayer $MoTe_2$. *ACS Nano* **2020**, *14*, 8299−8306.
(53) Qi, Y.; Naumov, P. G.; Ali, M. N.; Rajamathi, C. R.; Schnelle, W.; Barkalov, O.; Hanfland, M.; Wu, S.-C.; Shekhar, C.; Sun, Y.; Süß, V.; Schmidt, M.; Schwarz, U.; Pippel, E.; Werner, P.; Hillebrand, R.; Förster, T.; Kampert, E.; Parkin, S.; Cava, R. J.; Felser, C.; Yan, B.; Medvedev, S. A. Superconductivity in Weyl semimetal candidate $MoTe_2$. *Nat. Commun.* **2016**, *7*, 11038.
(54) Lezama, I. G.; Ubaldini, A.; Longobardi, M.; Giannini, E.; Renner, C.; Kuzmenko, A. B.; Morpurgo, A. F. Surface transport and band gap structure of exfoliated 2H-$MoTe_2$ crystals. *2D Mater.* **2014**, *1*, 021002.
(55) Takeuchi, O.; Yoshida, S.; Shigekawa, H. Light-modulated scanning tunneling spectroscopy for nanoscale imaging of surface photovoltage. *Appl. Phys. Lett.* **2004**, *84*, 3645−3647.
(56) Yoshida, S.; Kikuchi, J.; Kanitani, Y.; Takeuchi, O.; Oigawa, H.; Shigekawa, H. Tip-induced band bending and its effect on local barrier height measurement studied by light-modulated scanning tunneling spectroscopy. *e-J. Surf. Sci. Nanotechnol.* **2006**, *4*, 192−196.
(57) Attar, A. R.; Chang, H. T.; Britz, A.; Zhang, X.; Lin, M. F.; Krishnamoorthy, A.; Linker, T.; Fritz, D.; Neumark, D. M.; Kalia, R. K.; Nakano, A.; Ajayan, P.; Vashishta, P.; Bergmann, U.; Leone, S. R. Simultaneous observation of carrier-specific redistribution and coherent lattice dynamics in 2H-$MoTe_2$ with femtosecond core-level spectroscopy. *ACS Nano* **2020**, *14*, 15829−15840.
(58) Meckbach, L.; Hader, J.; Huttner, U.; Neuhaus, J.; Steiner, J. T.; Stroucken, T.; Moloney, J. V.; Koch, S. W. Ultrafast band-gap renormalization and build-up of optical gain in monolayer $MoTe_2$. *Phys. Rev. B* **2020**, *101*, 075401.
(59) Chi, Z.; Chen, H.; Chen, Z.; Zhao, Q.; Chen, H.; Weng, Y.-X. Ultrafast Energy Dissipation via Coupling with Internal and External Phonons in Two-Dimensional MoS_2. *ACS Nano* **2018**, *12*, 8961−8969.
(60) Britz, A.; Attar, A. R.; Zhang, X.; Chang, H. T.; Nyby, C.; Krishnamoorthy, A.; Park, S. H.; Kwon, S.; Kim, M.; Nordlund, D.; Sainio, S.; Heinz, T. F.; Leone, S. R.; Lindenberg, A. M.; Nakano, A.; Ajayan, P.; Vashishta, P.; Fritz, D.; Lin, M. F.; Bergmann, U. Carrier-specific dynamics in 2H-$MoTe_2$ observed by femtosecond soft x-ray absorption spectroscopy using an x-ray free-electron laser. *Struct. Dyn.* **2021**, *8*, 014501.
(61) Arashida, Y.; Umeda, N.; Mogi, H.; Ishikawa, M.; Hatanaka, A.; Takeuchi, O.; Yoshida, S.; Shigekawa, H. Phase-controllable multi-laser system with coaxially combined near-infrared and subcycle mid-infrared and THz pulsed beams. *Appl. Phys. Express* **2022**, *15*, 092006.

https://doi.org/10.1021/acsphotonics.2c00995
ACS Photonics 2022, 9, 3156−3164